JOURNAL OF APPLIED PHYSICS **97**, 114325 (2005)

Equilibrium limits of coherency in strained nanowire heterostructures

Elif Ertekin,[a] P. A. Greaney, and D. C. Chrzan
Department of Materials Science and Engineering, 210 Hearst Memorial Mining Building, University of California, Berkeley, California 94720-1760
and Materials Sciences Division, 1 Cyclotron Road, M.S. 66, Lawrence Berkeley National Laboratory, Berkeley, California

Timothy D. Sands[b]
School of Materials Engineering, School of Electrical and Computer Engineering, and Birck Nanotechnology Center, 501 Northwestern Avenue, Purdue University, West Lafayette, Indiana 47907-2044

(Received 10 December 2004; accepted 14 March 2005; published online 7 June 2005)

Due to their unique boundary conditions, nanowire heterostructures may exhibit defect-free interfaces even for systems with large lattice mismatch. Heteroepitaxial material integration is limited by lattice mismatches in planar systems, but we use a variational approach to show that nanowire heterostructures are more effective at relieving mismatch strain coherently. This is an equilibrium model based on the Matthews critical thickness in which the lattice mismatch strain is shared by the nanowire overlayer and underlayer, and could as well be partially accomodated by the introduction of a pair of misfit dislocations. The model is highly portable to other nanowire material systems and can be used to estimate critical feature sizes. We find that the critical radius of this system is roughly an order of magnitude larger than the critical thickness of the corresponding thin film/substrate material system. Finite element analysis is used to assess some aspects of the model; in particular, to show that the variational approach describes well the decay of the strain energy density away from the interface. © *2005 American Institute of Physics*.
[DOI: 10.1063/1.1903106]

I. INTRODUCTION

A better understanding of heteroepitaxial growth processes and interfacial defect formation has resulted in improvements to the quality of two-dimensional heteroepitaxial systems. In semiconductor heteroepitaxy, this has enabled developments in optoelectronic devices, light-emitting diodes, laser diodes, transistors, quantum-cascade lasers, and many other devices. Yet, heteroepitaxial integration of some semiconductor systems remains inaccessible due to large lattice mismatches between the materials of interest. A large lattice mismatch results in poor-quality interfaces with high misfit dislocation density; these dislocations influence the electrical behavior in several ways. For instance, they are preferred sites for impurity atoms, high-diffusivity paths for dopants, and nonradiative recombination centers. The Si/Ge heteroepitaxial system is one example where use of the interface as an active device component has remained largely out of reach due to the large 4% lattice mismatch. In the InAs/InP system, only a few atomic layers can be grown before islands or misfit dislocations form.

The recent demonstrations of coherent, lattice-mismatched nanowire semiconductor heterostructures[1–3] by the vapor-liquid-solid synthesis mechanism[4,5] represent the first foray into a distinct realm of heterojunction functionality and performance. These longitudinally heterostructured nanowires enable band gap engineering in one-dimensional structures, with potential applications towards unique quantum-dot geometries, *pn* and *pnp* junctions, nanowire superlattices, light-emitting devices, and thermoelectric devices. Other nanotube and nanowire interfaces have been fabricated using a variety of techniques.[6–13] Characterization of the electrical properties of these interfaces has included photoluminescence spectra[6] and current-voltage analysis.[8,9,11,13] Remarkably, we have not been able to find detailed analysis of the atomic structure of the interface, which we attribute to the relative recency in the fabrication of controlled, sharp interfaces (e.g., see Bjork *et al.*[2]). Yet, this is sure to follow soon as nanowire and nanotube interfaces work their way into the laboratory.

An important manner in which nanowire heterostructures differ from their planar counterparts is by their elastic boundary conditions: while a thin film is constrained laterally during growth, a nanowire can relieve strain energy via lateral relaxation. We expect that one-dimensional systems can be grown defect-free more readily than their two-dimensional counterparts, and thus they afford the opportunity to integrate classes of materials that, due to large mismatch, are not realizable in planar systems. The goal of this work is to explore this possibility quantitatively. The development of a simple model that describes coherency limits in strained heterostructured nanowires is then not only academically interesting, but it also can be useful to the band structure and device engineer.

Indeed, recently many scientists have noted the potential uses of nanostructures as a means of improving interface quality in heteroepitaxial systems.[1,2,14] Almost ten years ago, Luryi and Suhir[15] formulated expressions for the critical thickness for growth of strained heterolayers that include the

[a]Electronic mail: elif@berkeley.edu
[b]Electronic mail: tsands@ecn.purdue.edu

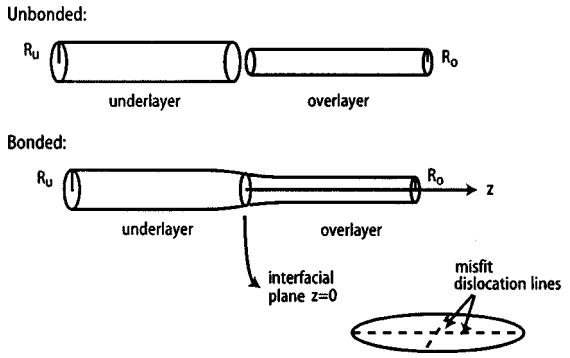

FIG. 1. Schematic of heterostructured nanowire, before and after interfacial bonding. The misfit dislocation geometry considered here is illustrated as well.

effects of the finite size of the substrate; they show that for small sizes, the strain energy is much reduced as a result of lateral relaxation away from the interface. This, idea has been extended to that of nanoheteroepitaxy,[16] in which epilayers are created by coalescense of an array of nanoscale islands epitaxially grown on lithographically patterned substrates. It is observed that misfit dislocation densities are reduced using this approach. Theoretical modeling of the principles of nanoheteroepitaxy is detailed in Zubia and Hersee.[17]

As the theoretical developments in two-dimensional heteroepitaxy have been useful in guiding interface engineering, we believe that the same will be true for one-dimensional systems. Thus, we present here a fundamental model, in the spirit of the Matthews model,[18] to predict the critical radius of a heterostructured nanowire system. Although the effects of lateral relaxation resulting from finite-size effects have been explored previously,[15,17] here we describe coherency limits specifically for the one-dimensional nanowire heterostructure (other models have been geared towards growth of thin films on patterned substrates or on the inclusion of finite-size effects on the strain fields in islands). It is quite likely that further refinements to our model will be made in the future, as greater experimental understanding of nanowire interfacial defects is gained. However, with this initial attempt, we obtain a glimpse into the nature of the one-dimensional heterostructure. Finite element analysis is used to support the variational framework that is developed. Most importantly, we demonstrate that, due to lateral relaxation at the boundaries, the one-dimensional heterostructure does offer advantages over conventional two-dimensional interfaces and is an avenue worth pursuing.

II. EQUILIBRIUM MODEL FORMULATION

A schematic of the heterostructured nanowire is shown in Fig. 1. The nanowire is oriented along the z axis and comprises an elastically isotropic underlayer and an elastically isotropic overlayer, with an interface at $z=0$. The unstrained (i.e., before interfacial bonding) radii of the underlayer and overlayer are denoted R_u and R_o, respectively. (Here and hereafter, subscripts and superscripts u and o denote the underlayer and the overlayer, respectively.) The lattice mismatch between the overlayer and the underlayer is denoted by f, where $f \geqslant 0$, and

$$R_o = (1-f)R_u. \tag{1}$$

The interface is created by bonding the two semi-infinite nanowires together at $z=0$, as illustrated in Fig. 1. The overlayer, occupying $z \geqslant 0$, $0 \leqslant r_o \leqslant R_o$, is "stretched" and the underlayer, occupying $z \leqslant 0$, $0 \leqslant r_u \leqslant R_u$, is "squeezed" so that the two nanowire cross sections are mapped onto each other at the interface. The mapping is coherent if misfit dislocations do not form, and semicoherent otherwise. The effective radius R_{eff} at the interface satisfies $R_o < R_{\text{eff}} < R_u$; its precise value depends on the relative values of the elastic (Lamé) parameters that describe the nanowires: λ_u, μ_u, λ_o, and μ_o. Far away from the interface in both the overlayer and underlayer, the nanowires can relax, and the radii approach R_o and R_u, respectively. (In the analysis that follows, we will characterize this relaxation by a relaxation distance α; we assume that both the underlayer and overlayer are long with respect to the relaxation distance α).

At a given lattice mismatch f, if the radii R_o and R_u are small, the circular cross section of the overlayer will be coherently mapped onto that of the underlayer without formation of misfit dislocations. The system is then elastically strained, but remains coherent at the interface. Ultimately, as the radii increase, the system loses its purely one-dimensional nature, and relaxation of the strain fields away from the interface is inhibited. For large lattice misfit or for particularly large R_o and R_u, misfit dislocations may arise to accomodate the mismatch strain. Thus, there is a critical overlayer radius R_o^*. For $R_o < R_o^*$, the interface will be coherent and the formation of misfit dislocations is not energetically favored; otherwise for $R_o > R_o^*$, misfit dislocations can form to relieve the mismatch strain. The goal of this work is to describe a model for $R_o^*(f)$, the critical radius as a function of lattice mismatch.

The development of this critical radius model roughly parallels the Matthews critical thickness model[18] for heterostructured thin-films. For a given mismatch f and overlayer radius R_o, the total strain energy in a coherent nanowire heterostructure is compared to the total energy (residual strain energy and dislocation energy) of a dislocated nanowire heterostructure. In the dislocated system, a small portion of the total mismatch f is accomodated by the dislocations, while the remainder (the *residual mismatch*) is accomodated by elastic strain in both the underlayer and overlayer. For small R_o, the coherent system has a lower energy; for large R_o, the dislocated system has a lower energy. The critical radius at which the transition occurs, R_o^*, is the radius at which the total energy for both systems is the same.

In this analysis, as with the Matthews model for epitaxial thin films, interactions between the dislocations and mismatch strain fields are not considered. The total strain energy is considered to be a superposition of the strain energy arising independently from the residual mismatch and from the dislocations themselves. This analysis is accurate only when dislocations account for only a small portion of the entire misfit strain (and thus is valid when determining the critical

size at which dislocations are first introduced). We restrict our analysis below to the introduction of only the first pair of misfit dislocations to avoid this (and other) complications.

A. Coherent nanowire heterostructure

We first wish to determine an expression for the elastic strain energy accomodated by the overlayer and the underlayer for a coherent system. Ideally, it should be possible to determine the exact solutions to the equations of elasticity describing the displacement, stress, and strain fields in the vicinity of the interface. These solutions are axially symmetric. They must as well meet the criterion that, when dislocation-free, the two cross sections at $z=0$ are *coherently* mapped onto each other, so that, using a cylindrical coordinate system, the displacements of the underlayer and overlayer satisfy

$$\left.\begin{aligned} u_z^o(r_u(1-f),z=0) &= u_z^u(r_u,z=0) \\ r_u(1-f)+u_r^o(r_u(1-f),z=0) &= r_u+u_r^u(r_u,z=0) \end{aligned}\right\} \quad 0\leqslant r_u\leqslant R_u, \tag{2}$$

where u_r^o denotes the radial displacements in the overlayer, u_z^o denotes the z displacements in the overlayer, u_r^u denotes the radial displacements in the underlayer, and u_z^u denotes the z displacements in the underlayer.

Also, the stress tensor components σ_{zz} and σ_{rz} are continuous across the interface so that

$$\left.\begin{aligned} \sigma_{zz}^o(r_u(1-f),z=0) &= \sigma_{zz}^u(r_u,z=0) \\ \sigma_{rz}^o(r_u(1-f),z=0) &= \sigma_{rz}^u(r_u,z=0) \end{aligned}\right\} \quad 0\leqslant r_u\leqslant R_u. \tag{3}$$

In addition to satisfying the constraints in Eqs. (2) and (3), the solutions must, as well, leave the free lateral surfaces traction-free:

$$\left.\begin{aligned} \sigma_{rr}^o(R_u(1-f),z) &= 0 \\ \sigma_{rz}^o(R_u(1-f),z) &= 0 \end{aligned}\right\} \quad z\geqslant 0;$$

$$\left.\begin{aligned} \sigma_{rr}^u(R_u,z) &= 0 \\ \sigma_{rz}^u(R_u,z) &= 0 \end{aligned}\right\} \quad z\leqslant 0. \tag{4}$$

Determining the exact solutions should be possible with a stress function approach or by using complex variable methods, but here we proceed instead by using a variational approach (principle of minimum potential energy) to obtain an expression for the strain energy in the coherent heterostructure. An advantage of this approach is that the critical radius model becomes a simple tool for the nanodevice engineer to predict the formation of interfacial defects.

We allow relaxation of *both* the underlayer and the overlayer, and assume the following relationship for the displacement fields:

$$u_r^o(r_o,z)=Br_o\exp\left[\frac{-z}{2\alpha R_o}\right],$$

$$u_r^u(r_u,z)=(B-f-fB)r_u\exp\left[\frac{z}{2\alpha(1-f)R_u}\right]\approx(B-f)r_u\exp\left[\frac{z}{2\alpha(1-f)R_u}\right],$$

$$u_z^o(r_o,z)=(Cr_o+DR_o)\exp\left[\frac{-z}{2\alpha R_o}\right],$$

$$u_z^u(r_u,z)=(C(1-f)r_u+D(1-f)R_u)\exp\left[\frac{z}{2\alpha(1-f)R_u}\right]\approx(Cr_u+DR_u)\exp\left[\frac{z}{2\alpha(1-f)R_u}\right]. \tag{5}$$

With this choice of radial displacements, the overlayer is uniformly stretched and the underlayer is uniformly squeezed. The fields u_z^o and u_z^u are incorporated to allow for relaxation in the z direction so that the planes of constant z are not held rigid. We assume that the fields decay exponentially with distance from the interface, with decay parameter $\alpha>0$, to reflect the strain energy relaxation that we expect to see in nanowires. Of course, these displacement fields are not self-equilibrated nor do they satisfy the free-surface tractions on the lateral surfaces (in the minimum potential energy approach, they need not); however the dimensionless variational parameters B, C, D, and α will be determined by energy minimization to best reflect the exact displacement fields. The displacements u_r^u and u_z^u in the underlayer are expressed in terms of parameters B, C, and D so that the conditions in Eq. (2) are satisfied to first order. [Note that in this formulation, we are neglecting the stress continuity constraints of Eq. (3)]. B, where $0\leqslant B\leqslant f$, indicates the degree of strain partitioning between the overlayer and the underlayer: for the case that the elastic parameters of the overlayer and underlayer (both assumed to be isotropic) are identical, we expect $B\approx f/2$; so that the overlayer (in tension) conforms to the underlayer (in compression) to the same extent that the underlayer conforms to the overlayer.

The stresses and strains in the overlayer can be determined. According to Hookean constitutive behavior, $\sigma_{ij}=C_{ijkl}\epsilon_{kl}$, where for isotropic materials $C_{ijkl}=\lambda\delta_{ij}\delta_{kl}+\mu(\delta_{ik}\delta_{jl}+\delta_{il}\delta_{jk})$ (summation convention implied). Thus we have from kinematics that

$$\epsilon_{rr}^o=B\exp\left[\frac{-z}{2\alpha R_o}\right],$$

$$\epsilon^o_{\theta\theta} = B \exp\left[\frac{-z}{2\alpha R_o}\right],$$

$$\epsilon^o_{zz} = -\frac{(Cr_o + DR_o)}{2R_o\alpha} \exp\left[\frac{-z}{2\alpha R_o}\right],$$

$$\epsilon^o_{rz} = \frac{-Br_o + CR_o\alpha}{4R_o\alpha} \exp\left[\frac{-z}{2\alpha R_o}\right] \tag{6}$$

and from the constitutive relations that

$$\sigma^o_{rr} = \frac{4(\lambda_o + \mu_o)BR_o\alpha - \lambda_o(Cr_o + DR_o)}{2R_o\alpha} \exp\left[\frac{-z}{2\alpha R_o}\right],$$

$$\sigma^o_{\theta\theta} = \frac{4(\lambda_o + \mu_o)BR_o\alpha - \lambda_o(Cr_o + DR_o)}{2R_o\alpha} \exp\left[\frac{-z}{2\alpha R_o}\right],$$

$$\sigma^o_{zz} = \frac{4\lambda_o BR_o\alpha - (\lambda_o + 2\mu_o)(Cr_o + DR_o)}{2R_o\alpha} \exp\left[\frac{-z}{2\alpha R_o}\right],$$

$$\sigma^o_{rz} = \frac{\mu_o(-Br_o + 2CR_o\alpha)}{2R_o\alpha} \exp\left[\frac{-z}{2\alpha R_o}\right]. \tag{7}$$

Similar expressions are obtained for the underlayer:

$$\epsilon^u_{rr} = (B - f)\exp\left[\frac{z}{2\alpha(1-f)R_u}\right],$$

$$\epsilon^u_{\theta\theta} = (B - f)\exp\left[\frac{z}{2\alpha(1-f)R_u}\right],$$

$$\epsilon^u_{zz} = \frac{(Cr_u + DR_u)}{2(1-f)R_u\alpha} \exp\left[\frac{z}{2\alpha(1-f)R_u}\right],$$

$$\epsilon^u_{rz} = \frac{(B-f)r_u + 2C(1-f)R_u\alpha}{4(1-f)R_u\alpha} \exp\left[\frac{z}{2\alpha(1-f)R_u}\right] \tag{8}$$

and

$$\sigma^u_{rr} = \frac{4(\lambda_o + \mu_o)(B-f)(1-f)R_u\alpha + \lambda_o(Cr_u + DR_u)}{2R_u\alpha} \times \exp\left[\frac{z}{2\alpha(1-f)R_u}\right],$$

$$\sigma^u_{\theta\theta} = \frac{4(\lambda_o + \mu_o)(B-f)(1-f)R_u\alpha + \lambda_o(Cr_u + DR_u)}{2R_u\alpha} \times \exp\left[\frac{z}{2\alpha(1-f)R_u}\right],$$

$$\sigma^u_{zz} = \frac{4\lambda_o(B-f)(1-f)R_u\alpha + (\lambda_o + 2\mu_o)(Cr_u + DR_u)}{2(1-f)R_u\alpha} \times \exp\left[\frac{z}{2\alpha(1-f)R_u}\right],$$

$$\sigma^u_{rz} = \frac{\mu_o((B-f)r_u + 2C(1-f)R_u\alpha)}{2R_u(1-f)\alpha} \exp\left[\frac{z}{2\alpha(1-f)R_u}\right]. \tag{9}$$

On the interfacial plane, the strains satisfy

$$|\epsilon^o_{rr}| + |\epsilon^u_{rr}| = |\epsilon^o_{\theta\theta}| + |\epsilon^u_{\theta\theta}| = |f| \tag{10}$$

to first order.

Let $e_o = e_o(r,z) = \frac{1}{2}\sigma^o_{ij}\epsilon^o_{ij}$ be the strain energy density in the overlayer and $e_u = e_u(r,z) = \frac{1}{2}\sigma^u_{ij}\epsilon^u_{ij}$ be the strain energy density in the underlayer. The total strain energy in the overlayer E_o and in the underlayer E_u can be obtained by integration:

$$E_o = \int_0^\infty \int_0^{2\pi} \int_0^{R_o} e_o(r_o,z) r_o dr_o d\theta dz$$

$$= \frac{\pi R_o^3}{48\alpha}[\lambda_o(3C^2 + 8C(D - 4B\alpha) + 6(D - 4B\alpha)^2) + \mu_o(-16BC\alpha + B^2(3 + 96\alpha^2) + 2(3C^2(1 + 4\alpha^2) + 8CD + 6D^2))] \tag{11}$$

and

$$E_u = \int_{-\infty}^0 \int_0^{2\pi} \int_0^{R_u} e_u(r_u,z) r_u dr_u d\theta dz$$

$$= \frac{\pi R_o^3}{48(1-f)^4\alpha}[\lambda_u(3C^2 + 8C(D + 4(B-f)(1-f)\alpha) + 6(D + 4(B-f)(1-f)\alpha)^2) + \mu_u(16C(B-f) \times (1-f)\alpha + (B-f)^2(3 + 96(1-f)^2\alpha^2) + 2(8CD + 6D^2 + 3C^2(1 + 4(1-f)^2\alpha^2)))]. \tag{12}$$

The total elastic energy $E_{el} = E_o + E_u$ must then be minimized with respect to the parameters α, B, C, and D. We can solve for the energy-minimizing decay constant α^* in terms of the other parameters by solving $\partial/\partial\alpha(E_{el}) = 0$, which gives

$$\alpha^* = (6B^2\mu + 3f^2\mu + 3fB\mu(-2 + B(-2 + f)(2 + (-2 + f)f)) + (3C^2 + 8CD + 6D^2)(2 + f(-2 + f)(2 + (-2 + f)f))(\lambda + 2\mu))^{1/2}/2\sqrt{6}(1-f)\sqrt{4f(f-2B)(\lambda+\mu) + (2 + f(-2+f))(\mu C^2 + 4B^2(\lambda+\mu))}. \tag{13}$$

Here and hereafter, we assume that $\lambda_o = \lambda_u = \lambda$ and $\mu_o = \mu_u = \mu$. It is possible to carry through the analysis without this assumption, but the algebra becomes substantially more tedious while not qualitatively altering the results. (For particularly

large elastic mismatches, it may be desirable as well to consider distinct relaxation parameters α_o and α_u for the overlayer and underlayer.) Substitution of Eq. (13) into the expression for E_{el} gives

$$E_{\mathrm{el}} = \frac{\pi R_o^3}{12(1-f)^3}(4f(B(3+f(-3+f))-1)(3D\lambda + C(2\lambda+\mu)) + \sqrt{6}\sqrt{(4f^2-8Bf)(\lambda+\mu)+(2+f(-2+f))(C^2\mu+4B^2(\lambda+\mu))} \times \sqrt{(\lambda+2\mu)(2+f(-2+f)(2+f(-2+f)))(3C^2+8CD+6D^2)}). \quad (14)$$

Of course, this must be minimized with respect to the parameters B, C, and D, which set the topology of the interface. We do this minimization numerically, and denote the energy-minimizing parameters as B^*, C^*, and D^*, corresponding to the elastic energy E_{el}^*, so that

$$E_{\mathrm{el}}^* = E_{\mathrm{el}}\big|_{B=B^*,C=C^*,D=D^*}. \quad (15)$$

We show in Sec. IV via finite element analysis that this provides a good estimate for the strain energy in the heterostructure (overestimates the strain energy by approximately 15%).

B. Energy of misfit dislocations

It is difficult to determine *a priori* the favored misfit dislocation configuration in a heterostructured nanowire. The Matthews model for planar thin films more easily accomodates cubic systems of rectangular cross section, where the introduction of a perpendicular pair of misfit dislocations uniformly alters the residual lattice mismatch in both the x and y directions. Misfit dislocations in cubic thin-film heterostructures are often observed to arise in this manner, so the model is well justified for those systems. As far as we know, misfit dislocations have not yet been observed in nanowire heterostructures. In nanowires, as in thin films, the most likely dislocation configuration should depend on the crystal structure and orientation. For convenience, we will study the formation of a pair of misfit dislocations as illustrated in Fig. 1. This is not the first time that such a geometry has been considered; for instance, see Cabrera,[19,20] who used a similar geometry to consider misfit dislocations in islands. It is important to note that this is not necessarily the favored dislocation configuration. For instance, in systems that have three-or sixfold crystal symmetry along the wire axis, a perpendicular pair is unlikely. The first dislocation in GaN, for instance, might be an edge partial, since the stacking fault energy is low. However, the configuration that we have selected makes the analysis amenable to a simple critical radius model.

Misfit dislocations in the heterostructured nanowire system introduce both a core energy and a strain energy. In planar heterostructured systems with face-centered-cubic lattice structures in {111} or {100} orientation, misfit dislocations are often introduced from the surface via the {111} glide planes. These dislocations have both edge and screw components, but only the edge component of the dislocation reduces misfit strain. In nanowire heterostructures, the geometry is likely to permit pure edge dislocations due to the available slip plane that is coincident with the interface and intersecting the nanowire surface. Thus, we assume pure edge dislocations in this model.

We denote the number of dislocation pairs by n, such that $n=0$ corresponds to a completely coherent system, and $n=1$ corresponds to a system containing one pair of perpendicular edge dislocations. As the formation of the first dislocation is the critical event for a semiconductor material, we are concerned with the transition from the $n=0$ to the $n=1$ configuration. If we denote the Burger's vector for each misfit dislocation in the overlayer as b (so that for the two dislocations we have $\vec{b}_1 = b\hat{x}$ and $\vec{b}_2 = b\hat{y}$), then the residual radial misfit strain (that is, the strain not accomodated by the dislocation) is

$$|f_{\mathrm{res}}| = |f| - |\epsilon_d| = |f| - \left|\frac{nb}{2R_o}\right|. \quad (16)$$

We limit our analysis to $0 \leqslant b \leqslant 2R_o f$ so that the dislocation cannot overcompensate for the mismatch strain f.

The strain energy per unit length of an edge dislocation of Burger's vector b in an infinite medium is given by

$$\frac{W}{L} = \frac{b^2}{2\pi}\frac{\mu(\lambda+\mu)}{(\lambda+2\mu)}\ln\left(\frac{R\beta}{b}\right), \quad (17)$$

where R is the outer cutoff distance for the strain field and β is the core energy factor introduced to accomodate the nonlinearities near the dislocation core.[21] From this, we assume that the strain energy arising from n perpendicular dislocation pairs ($n=0$ or $n=1$) in the overlayer may be described by:

$$E_{\mathrm{disl}}^n = 2n(2R_o)\frac{b^2}{2\pi}\frac{\mu_o(\lambda_o+\mu_o)}{\lambda_o+2\mu_o}\ln\left(\frac{R_o\beta}{b}\right), \quad (18)$$

where we have taken the radius of the overlayer as the cutoff for the strain fields. Because we are accounting for the free surface only by introducing an outer cutoff for the strain fields, Eq. (18) overestimates somewhat the strain energy of the dislocation pair. This may, to some degree, offset the effects of the overestimate to the residual strain energy.

C. Critical radius

For a system containing $n=(0,1)$ dislocation pairs, the total excess energy (residual elastic strain energy and dislo-

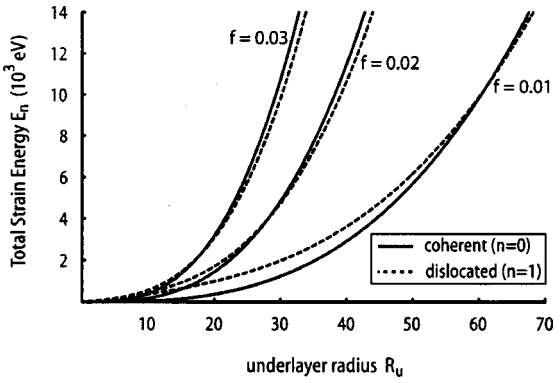

FIG. 2. Energy E_n, $n=(0,1)$, vs underlayer radius R_u for nanowire heterostructures with lattice mismatch $f=0.01,0.02,0.03$. $\beta=4$, $b=0.23$ nm, $\lambda_o=\lambda_u=60$ GPa, and $\mu_o=\mu_u=60$ GPa.

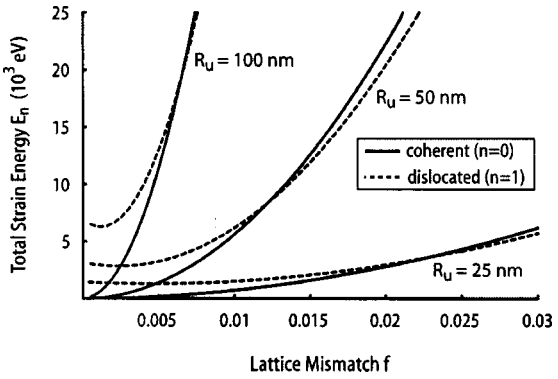

FIG. 3. Energy E_n, $n=(0,1)$, vs lattice mismatch f for nanowire heterostructures with underlayer radius $R_u=25,50,100$ nm. $\beta=4$, $b=0.23$ nm, $\lambda_o=\lambda_u=60$ GPa, and $\mu_o=\mu_u=60$ GPa.

cation energy) is obtained by combining Eqs. (15) and (18), noting that now in Eq. (15), $f\rightarrow f_{\text{res}}$ and substituting Eq. (16) for f_{res}

$$E_n = E_{\text{el}}^* + E_{\text{disl}}^n. \tag{19}$$

The residual mismatch f_{res} is used instead of f as now only a portion of the total mismatch f is accomodated "coherently" (for the completely coherent case, $f_{\text{res}}=f$; when a dislocation is present, f_{res} represents the residual mismatch that must be accomodated).

We can use Eq. (19) to compare energies of systems that are coherent or dislocated. The critical radius R_o^* is determined by setting $E_0=E_1$ and numerically solving for R_o. This is the nanowire analog to the transcendental expression obtained using a total energy approach to critical thicknesses in thin films. Many such thin-film equations have been obtained by various authors, we cite here the one described by Nix[22] because it most closely parallels our formulation:

$$d^* = \frac{b}{8\pi f(1+\nu)} \ln\left(\frac{\beta d^*}{b}\right), \tag{20}$$

where d^* is the critical thickness and ν is the Poisson is ratio for the thin film.

As a final note, in a more accurate formulation of the critical thickness model (both this model *as well as* the Matthews model), the strains arising from the dislocations and the residual misfit should be added together rather than the strain energies themselves in Eq. (19). The error that results from adding *strain energies* rather than *strains* is small when the strain relieved by the dislocation is small compared to the misfit strain, and is also small in the case that the dislocation energy is highly concentrated in the vicinity of the core.

III. RESULTS AND DISCUSSION

This analysis can be used to determine whether the coherent or dislocated configuration is preferred for a given heterostructured nanowire.

A. Critical radius of heterostructured nanowires

Figure 2 illustrates the dependence of E_n, $(n=0,1)$ vs R_u for systems with lattice mismatch $f=0.01,0.02,0.03$, respectively. The figures were generated using Eq. (19) with parameters typical of semiconducting materials: $\beta=4$, $b=0.23$ nm, $\lambda_o=\lambda_u=60$ GPa, and $\mu_o=\mu_u=60$ GPa.

In Fig. 2, the solid line corresponds to the energy of a coherent system (no dislocations), while the dashed line depicts the energy of a system with one dislocation pair. In all cases illustrated ($f=0.01,0.02,0.03$), for sufficiently small R_u, the coherent structure has lower energy. However, as R_u increases, the mismatch strain energy grows. Eventually, it becomes favorable to reduce the mismatch strain at the cost of introducing a misfit dislocation. The critical radii at which this occurs is, according to Fig. 2, $R_u^*\approx 60,25,15$ nm, respectively, for $f=0.01,0.02,0.03$. As expected, R_u^* decreases with increasing mismatch f. By comparison, the critical thickness of the same material system in thin-film geometry is $d^*\approx 2.86,1.07,0.55$ nm for $f=0.01,0.02,0.03$, respectively, according to Eq. (20). As a rough estimate, it appears that for a given lattice mismatch f, the critical radius of the nanowire heterostructure is approximately an order of magnitude (or more) larger than the critical thickness of the equivalent planar heteroepitaxial system.

Figure 3 shows the total strain energy E_n, $n=(0,1)$ versus lattice mismatch f for nanowire heterostructures with underlayer radii $R_u=25,50,100$ nm. This figure was generated using Eq. (19) as well, using the same material parameters as with Fig. 2. The solid and dashed lines again correspond to coherent and dislocated systems, respectively. We see from this figure that a nanowire with overlayer radius $R_u=25$ nm can accomodate mismatch strains up to the critical value $f^*=0.023$ before misfit dislocations are introduced. For nanowires with larger diameters, the ability to laterally relax to relieve mismatch strain becomes inhibited, so that misfit dislocations appear at lower values of the lattice mismatch. Thus, the critical value of the mismatch drops to $f^*\approx 0.013$ for $R_u=50$ nm and $f^*\approx 0.007$ for particularly large nanowires, $R_u=100$ nm.

It is significant to note that the critical radii so obtained are typically large compared to the wavelength of an electron (as shown in the next section); therefore, the range of compositions, and hence band gaps, over which heterostructures may be engineered is not limited by quantum confinement.

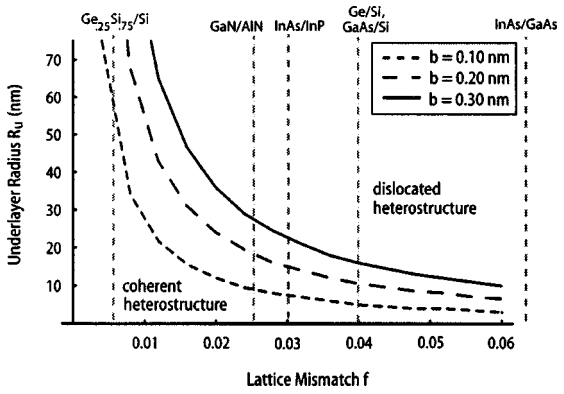

FIG. 4. Equilibrium diagram illustrating regions in (f, R_u) space for which the coherent and dislocated nanowire heterostructures are stable with respect to each other. $\beta=4$, $\lambda_o=\lambda_u=60$ GPa, and $\mu_o=\mu_u=60$ GPa.

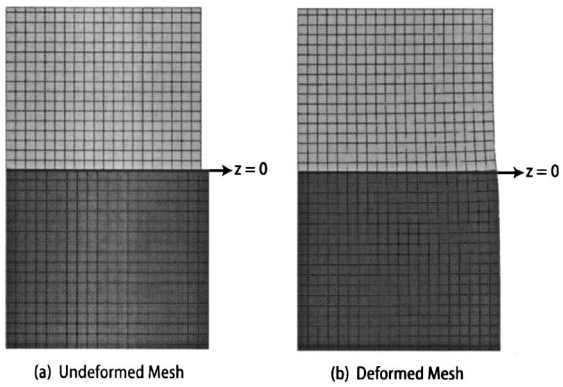

FIG. 5. Finite element mesh of heterostructured nanowire system, before and after bonding of interface. $f=0.04$, $\lambda_o=\lambda_u=60$ GPa, and $\mu_o=\mu_u=60$ GPa.

B. Equilibrium diagrams for heterostructured nanowires

To further explore the relationship between R_o^* and mismatch f, we have used Eq. (19) to construct the equilibrium diagram shown in Fig. 4. Each curve (corresponding to a particular Burger's vector b) represents the locus of intersections in (R_u, f) space between the curves E_1 and E_0. The region to the left of each curve is the coherent region, and the region to the right is incoherent. We used the same parameters as before: $\beta=4$, $\lambda_o=\lambda_u=60$ GPa, and $\mu_o=\mu_u=60$ GPa, but we illustrate the cases $b=0.1, 0.2, 0.3$ nm. For reference, we have marked the lines corresponding to the lattice mismatch associated with some common heteroepitaxial systems. The behavior captures the essential characteristics described above: small R_u enables lateral relaxation of the nanowire, and thus large mismatches f can be accomodated, while maintaining a coherent interface. Larger R_u restricts lateral relaxation, resulting in a decrease in the maximum mismatch that can be coherently accomodated.

According to Fig. 4, dislocations with larger b are admitted into the system only for larger mismatches f or larger radii R_o. If dislocations with small Burger's vectors are likely to form, then they can be introduced at smaller mismatches and smaller nanowire radii. Since the Burger's vector is usually dictated by the crystal structure and lattice parameters, the critical radius then depends on the specific material system itself rather than simply on the mismatch and the elastic parameters.

Lastly, we note that the critical radii shown in Fig. 4 are generally in agreement with the critical thicknesses presented in Zubia and Hersee.[17] Zubia and Hersee[17] considers the effect of finite lateral extent on the *critical thickness*. Despite this distinction, it is good that for sufficiently thick epilayers, the region in (R_u, f) space at which the energies become comparable in Zubia and Hersee[17] corresponds well to the critical radii as determined by our approach.

IV. CRITICAL ANALYSIS OF MODEL

In this section, we address some of the assumptions and limitations of the model. As with most critical thickness models, the total energy curves for the coherent (E_0) and dislocated (E_1) structures deviate by only a small fraction of their total value (Figs. 2 and 3). Thus, small adjustments to the model can result in substantial changes to the predicted critical radius. While this is indeed the case, we do believe that the trends exhibited in Figs. 2–4 capture the system's behavior.

A. Finite element analysis

Our variational formulation assumes a very particular form for the displacements in both the underlayer and overlayer. We have used the Finite Element Analysis Program (FEAP),[23] to determine the actual displacements, stresses, and strains within the nanowire so that we can compare it to our expression (15). Stress and strain distributions in epitaxial systems have been explored with finite element analysis previously, for instance Johnson and Freund[24] have used a similar approach to determine strain energies of islands grown epitaxially on substrates. The finite element approach that we implemented uses a two-dimensional (2D) axisymmetric model of the nanowire heterostructure. A portion of the as-constructed mesh (near the interface) is illustrated in Fig. 5(a). The upper region $z>0$ contains the overlayer, and the lower region $z<0$ contains the underlayer. The meshes are initially defined so that the radii of the overlayer and underlayer are unstrained (unbonded); for a given mismatch f, they are related by Eq. (1). The cuts $z=0$ on both the overlayer and underlayer are divided into an equal number of evenly spaced quadrilateral elements. An initial displacement $u_r \sim r$ is imposed on the nodes at the overlayer surface $z=0$ so that these nodes are mapped on to the corresponding nodes of the underlayer surface $z=0$. The two surfaces are thus coherently linked together, and then, in dynamic solution mode, the heterostructure is allowed to relax. The relaxed image is shown in Fig. 5(b).

We studied the displacements, stresses, and strains for the fully relaxed heterostructure for lattice mismatches $0 \leqslant f \leqslant 0.06$ and for a variety of material parameters to ensure that our variational approach gives a reasonable estimate of the strain energy. Examples of the stress distributions that we obtained for one particular case are illustrated in Fig. 6. Our variational form for the displacements results in an exponentially decaying strain energy density (with decay parameter α) with coordinate z. To assess this, the strain energy densi-

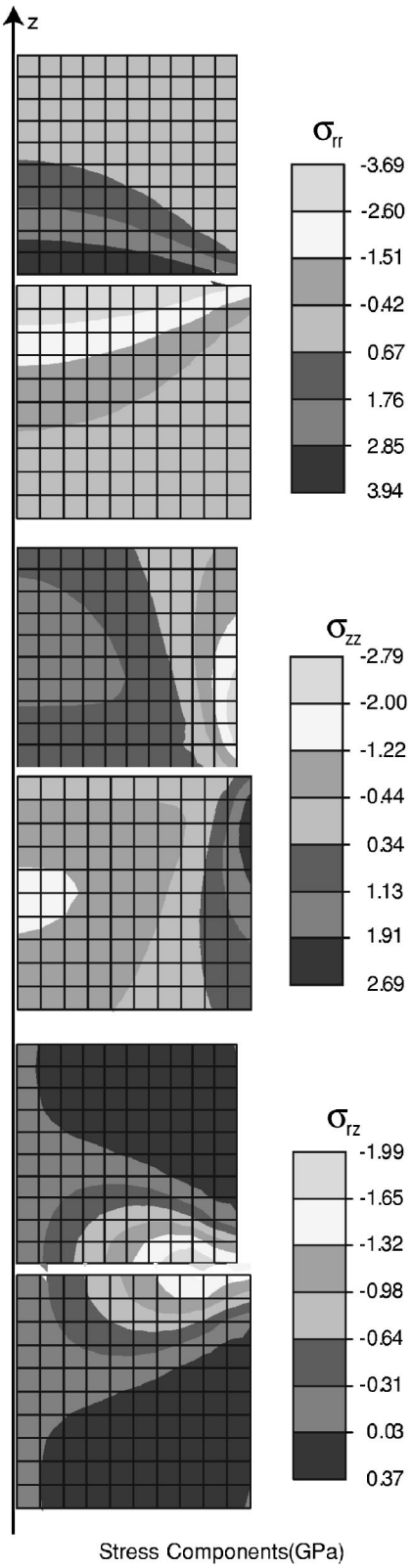

FIG. 6. Stress fields σ_{rr}, σ_{zz}, and σ_{rz} induced in heterostructred nanowire system, obtained via finite element analysis. $f=0.04$, $\lambda_o=\lambda_u=60$ GPa, and $\mu_o=\mu_u=60$ GPa.

ties from finite element analysis have been fitted to exponential functions. The fit as well as the actual data points as obtained from finite element methods is illustrated in Fig. 7 for various lattice mismatches. The magnitude of the decay parameters α for these systems are plotted in Fig. 8. It is

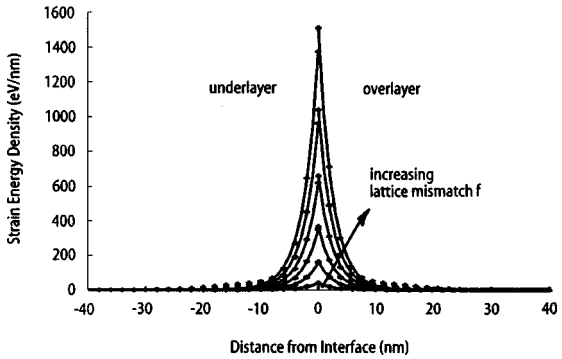

FIG. 7. Strain energy density in overlayer and underlayer for $f=0.01, 0.02, 0.03, 0.04, 0.05, 0.06$. Finite element results are indicated by the marker +; exponential fits to the finite element data are indicated by solid lines. $R_u=20$ nm, $\lambda_o=\lambda_u=60$ GPa, and $\mu_o=\mu_u=60$ GPa.

clear that α obtained from our approach [using B^*, C^*, and D^* in Eq. (13)] corresponds quite well to the strain energy decay constant as obtained by finite elements (this differs from the decay constant reported in Ref. 25 due to a typographical error in Ref. 25, wherein rather than $\alpha=0.375$, we should have $2/(\alpha R_o)=0.375$, with $R_o=20$ nm.). These figures illustrate that (not surprisingly) α is not, to first order, a strong function of the lattice mismatch f. It does vary slightly with material parameters, but even these variations are quite small. The notion that nanowires with larger radii are less capable of relaxing laterally to relieve mismatch strain is supported by the demonstration that the decay constants are relatively constant over the range of systems studied.

In Fig. 9, we compare the displacements u_r^o and u_z^o at the interface from our variational approach to those obtained by finite element analysis. Our representation of the radial displacement u_r^o is quite good, and both our variational approach and finite element analysis results affirm that the mismatch strain is nearly equally partitioned between the overlayer and underlayer ($B^* \approx f/2$). Our representation for u_z^o is not nearly as good, however. It is possible to improve this by choosing a form for u_z^o and u_z^u with more degrees of freedom, thus allowing the system to relax more effectively via z displacements.

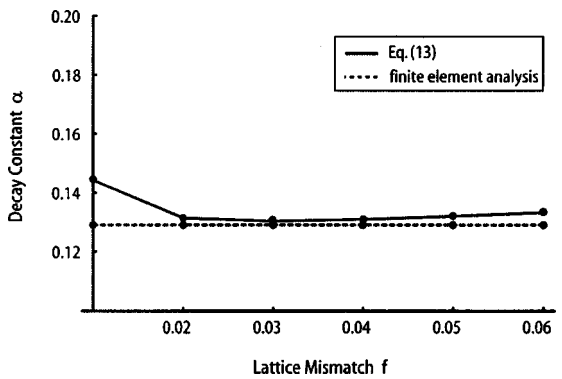

FIG. 8. Decay constant α for $f=0.01, 0.02, 0.03, 0.04, 0.05, 0.06$, as determined by finite element analysis and Eq. (15). $\lambda_o=\lambda_u=60$ GPa and $\mu_o=\mu_u=60$ GPa.

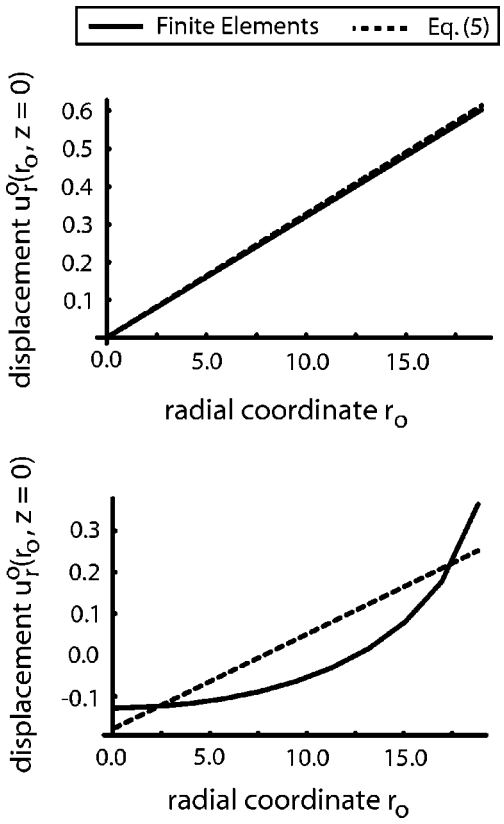

FIG. 9. Comparison between finite elements and Eq. (5) using B^*, C^*, and D^* of radial and z displacements in the overlayer at the interface. R_u =20 nm, $\lambda_o=\lambda_u=60$ GPa, $\mu_o=\mu_u=60$ GPa, and $f=0.06$.

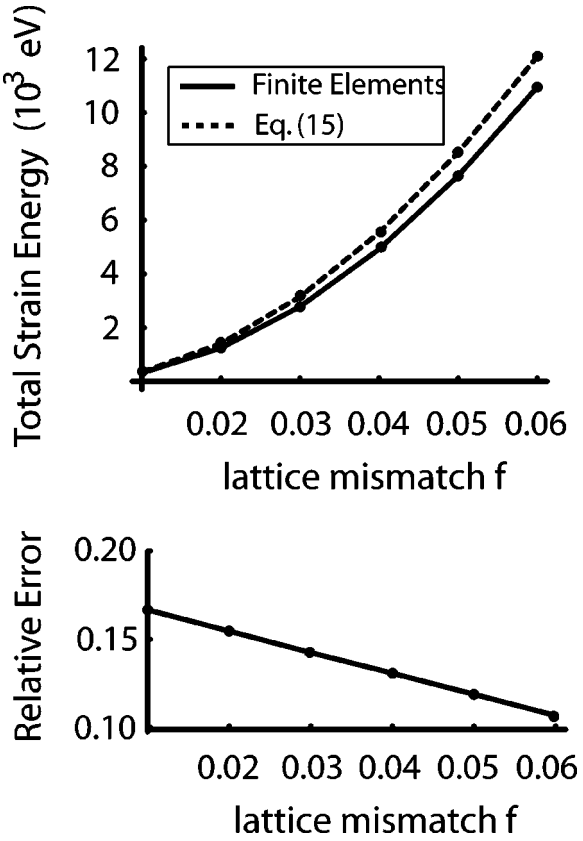

FIG. 10. Total strain energy in coherent nanowire heterostructure as a function of f according to Eq. (15) is compared with the total strain energy computed with finite element analysis for the cases $f=0.01, 0.02, 0.03, 0.04, 0.05, 0.06$. $R_u=20$ nm, $\lambda_o=\lambda_u=60$ GPa, and $\mu_o=\mu_u=60$ GPa.

Our variational approach takes no account of the stress continuity constraints at the interface [Eq. (3)]. Interestingly enough, our approach gives near continuity of σ_{rz} across the interface, while σ_{zz} at the interface is practically equal and opposite in the overlayer and underlayer. We suspect that the actual value of σ_{zz} in the interface should be zero, such that it changes sign at a given point from the overlayer to the underlayer (this can be seen in Fig. 6).

In Fig. 10, the strain energy as computed from finite element analysis is compared to the strain energy as given by Eq. (15) for various lattice mismatches f. As Fig. 10 implies, our results are reasonable. The relative error in our expression decreases with the lattice mismatch f, but always remains within $\approx$20% for all f considered here (the larger errors at small mismatch may be caused by difficulties in computing numerically the smaller strain energies). The largest contribution to this error arises most likely from the displacements u_z^o and u_z^u and the unrelaxed lateral surfaces.

B. Kinetic considerations

This model, and the Matthews model, are equilibrium models that do not consider kinetic barriers to dislocation introduction. Often, in planar heterostructures, thin films are grown dislocation-free well beyond the critical thickness because of the high-energy barriers to dislocation introduction. These planar heterostructures remain in a metastable coherent state.[26,27] Kinetics may be a consideration in heterostructured nanowires as well. However, in nanowire heterostructures, the interface itself is often a slip plane that intersects the free surface—kinetic barriers may be less significant here than in thin-film systems. Thus, an equilibrium model for nanowires may be even more relevant than it's planar counterpart. Alternatively, the surfaces may not be ready sources for dislocations; this remains to be seen.

V. CONCLUSIONS

We have adapted the critical thickness model of Matthews to study equilibrium and coherency limits in one-dimensional heterostructures for which lateral relaxation is allowed at the boundaries. The results of our model indicate that the adoption of the nanowire geometry yields critical radii that are roughly an order of magnitude larger than the critical thickness of the same substrate-thin film system. The implication is that the nanowire geometry should enable integration of disparate classes of materials that cannot be realized in planar systems at equilibrium. These results can serve as a guide for band structure engineering of nanowire heterostructures.

ACKNOWLEDGMENTS

This work is supported by the National Science Foundation under Grant Nos. CTS-010360, EEC-0085569, and ECS-0424161. Additional support was provided by the Directorate, Office of Basic Energy Sciences of the Department

of Energy under Contract No. DE-AC03-76SF00098. Support has also been provided by the National Science Foundation under Grant No. ECS-0424161.

[1]Y. Wu, R. Fan, and P. Yang, Nano Lett. **2**, B3 (2002).
[2]M. Bjork *et al.*, Nano Lett. **2**, 87 (2002).
[3]M. Gudiksen, L. Lauhon, J. Wang, D. Smith, and C. Lieber, Nature (London) **415**, 617 (2002).
[4]R. Wagner and W. Ellis, Appl. Phys. Lett. **4**, 89 (1964).
[5]R. Wagner and W. Ellis, J. Met. **16**, 761 (1964).
[6]K. Haraguchi, T. Katsuyama, and K. Hiruma, J. Appl. Phys. **75**, 4220 (1994).
[7]Y. Zhang, T. Ichihashi, E. Landree, F. Nihey, and S. Iijima, Science **285**, 1719 (1999).
[8]J. Hu, M. Ouyang, P. Yang, and C. Lieber, Nature (London) **399**, 48 (1999).
[9]N. Kovtyukhova, B. Martin, J. Mbindyo, P. Smith, B. Razavi, T. S. Mayer, and T. E. Mallouk, J. Phys. Chem. B **105**, 8762 (2001).
[10]S. R. Nicewarner-Peña *et al.*, Science **294**, 137 (2001).
[11]Z. Yao, H. Postma, L. Balents, and C. Dekker, Nature (London) **402**, 273 (1999).
[12]P. D. Markowitz, M. P. Zach, P. C. Gibbons, R. M. Penner, and W. E. Buhro, J. Am. Chem. Soc. **123**, 4502 (2001).
[13]C. Zhou, J. Kong, E. Yenilmez, and H. Dai, Science **290**, 1552 (2000).
[14]L. Freund and T. Gosling, Appl. Phys. Lett. **66**, 1822 (1995).
[15]S. Luryi and E. Suhir, Appl. Phys. Lett. **49**, 140 (1986).
[16]S. D. Hersee *et al.*, IEEE J. Quantum Electron. **38**, 1017 (2002).
[17]D. Zubia and S. D. Hersee, J. Appl. Phys. **85**, 6492 (1999).
[18]J. Matthews, J. Vac. Sci. Technol. **12**, 126 (1975).
[19]N. Cabrera, Surf. Sci. **2**, 320 (1964).
[20]N. Cabrera, Mem. Sci. Rev. Metall. **62**, 205 (1965).
[21]*Theory of Dislocations*, 2nd ed., edited by J. P. Hirth and J. Lothe (Krieger, Malabar, FL, 1982).
[22]W. D. Nix, Metall. Trans. A **20**, 2217 (1989).
[23]O. C. Zienkiewicz and R. L. Taylor, *The Finite Element Method*, 5th ed. (Butterworth–Heinemann, Oxford, 2000), Vols. 1–2.
[24]H. Johnson and L. Freund, J. Appl. Phys. **81**, 6081 (1997).
[25]E. Ertekin, P. A. Greaney, T. D. Sands, and D. C. Chrzan, Mater. Res. Soc. Symp. Proc. **737**, 769 (2002).
[26]R. Hull and J. Bean, Appl. Phys. Lett. **54**, 925 (1989).
[27]B. Dodson and Y. Tsao, Appl. Phys. Lett. **51**, 1325 (1987).